Integration of multi-source geospatial data from GNSS Receivers, Terrestrial Laser Scanners, and Unmanned Aerial Vehicles

P. S. Dąbrowski[a]*, C. Specht[a] , M. Specht[b] , P. Burdziakowski[c] , A. Makar[d] and O. Lewicka[a]

[a]Department of Geodesy and Oceanography, Gdynia Maritime University, Gdynia, Poland; [b]Department of Transport and Logistics, Gdynia Maritime University, Gdynia, Poland; [c]Department of Geodesy, Gdansk University of Technology, Gdansk, Poland; [c]Department of Navigation and Hydrography, Polish Naval Academy, Gdynia, Poland

Corresponding author: Pawel S. Dabrowski, e-mail: p.dabrowski@wn.umg.edu.pl

ORCID:

0000-0002-6177-0493 - P. S. Dąbrowski

0000-0001-5631-6969 - C. Specht

0000-0002-6026-306X - M. Specht

0000-0002-2869-5727 - P. Burdziakowski

0000-0001-7121-5322 - A. Makar

Word count: 6456

Integration of multi-source geospatial data from GNSS Receivers, Terrestrial Laser Scanners, and Unmanned Aerial Vehicles

The analysis based on geospatial data from different measurement systems now constitutes a complex numerical and practical enterprise. The dynamic development of modern technologies enables rapid and precise acquisition of such data. Nonetheless, the diversity of reference systems is today one of the main challenges for their correct interpretation. The combined use of the processed measurement results and archival data in paper form constitutes an important direction for the development of this discipline. This issue is visible during the implementation of complex hydrographic and geodetic surveys requiring geospatial integration of results. The publication presents both the theoretical basis and the practical verification of the adopted methodology. The research material comes from the measurement campaign conducted to determine geospatial parameters for the tombolo phenomenon in Sopot. The results of differential GNSS RTK measurements, terrestrial laser scanning, bathymetric survey, photogrammetry, and analog archival bathymetric map were subjected to the integration process. The effectiveness of the presented procedure was confirmed by the obtained error estimators of values not exceeding three centimeters.

Introduction

There are many ways to determine the position of objects in space. Depending on the type of spatial data and its purpose, local and global reference systems are used (**Hofmann-Wellenhof et al. 2003**). Local systems can be divided into systems with known geometric parameters, which link them directly to global systems and undetermined local systems. The first group of local systems includes cartographic mappings (**Bugayevskiy and Snyder 2013**), in which the mapping functions take curvilinear spherical or ellipsoidal coordinates as arguments and then transform them from a three-dimensional space into a flat, two-dimensional map plane (**Yang et al. 1999**). The location of objects on the Earth's surface is indicated on the map by flat Cartesian coordinates. The basic property of the mapping functions is the unambiguous assignment of a point from the original surface (Earth) to one point on the surface of the image (map) (**Maling 1992**). This dependence also works the other way round, hence the spatial relation of the local system of map coordinates to the global earth system can be derived from the cartographic mapping formulas. Another group distinguished within local systems are undetermined systems, which do not have unambiguously determined, constant spatial relationships to the global systems. An example of an undetermined local system included coordinate systems in which geodetic measuring devices such as, e.g. tachometers or laser scanners operate (**Deumlich 1982**).

There are many ways in which spatial object data can be presented and described. Analogue studies in the form of paper maps have been known for several thousand years (**Robinson et al. 1978**). The rapid development of geodesy and measurement techniques initiated in the seventeenth and eighteenth centuries resulted in a rapid increase in the accuracy of maps and a shift from undetermined local studies to advanced cartographic mapping. Since then, thanks to known mapping function

formulas and representations of the meridians and parallels on maps, it has been possible to relate the map content to the global system **(Smith 1997)**. Another revolutionary step in cartography and spatial information system included the use of advanced tools and software based on numerical maps. The use of computers in cartography, digitalisation, and vectorisation of paper maps was another milestone in the use of archival analogue imaging **(Visvalingam 1990)**. Please note that it was not until the creation of a numerical equivalent of a map in raster or vector form that coordinate transformation processes became possible. This made it possible to use the imaging content in any coordinate system chosen by the user.

When using maps, we are dealing with the secondary acquisition of information about presented objects. A map is a representation of the field situation in a specific moment in the past **(Bagrow 2010)**. A different approach includes conducting measurements and recording observations with the use of surveying instruments. This process is an active form of expression of geospatial dependencies in the surrounding environment. During the measurement, a surveyor determines the current position of objects in the system of coordinates of the measuring instrument **(Deumlich 1982)**. In many cases, these very data are later on placed on maps. A system of coordinates implemented by a tachometer or laser scanner constitutes an undetermined local system **(Vosselman and Maas 2010)**. This means that the spatial relationships between the measured objects and the device are expressed with great accuracy **(Specht et al. 2016)**. In this case, however, there is no clear assignment of the obtained set of spatial information to a specific location on the Earth's surface and no indication of the proper (real) azimuth.

The problem of indeterminate systems of coordinates of geodetic devices has been solved by creating geodetic control networks. Initially, geo-referencing of the

network was performed through precise astronomical and geodetic measurements **(Torge and Müller 2012)**. In the last several decades it was common practice to determine the coordinates of geodetic control points based on global satellite navigation systems (GNSS). Apart from the complex methodology of computational processes, it should be noted that points included in the network constitute the physical realisation of reference systems through the determination of their three-dimensional orthocartesian (x, y, z) and curvilinear (B, L, h) coordinates **(Krynski et al. 2019)**. Based on known coordinates of the geodesic control points, surveyors relate the performed measurements and recorded observations to a given system of coordinates **(Dąbrowski et al. 2019)**. Please note that spatial data on the geodetic control networks are not always publicly available. In many situations, access to this data is limited by national legislation. Therefore, a reference to the results of tachometric and laser measurements to the points of the network results in the possibility of expressing the position of recorded objects in the coordinate system of the network.

In recent years, a separate discipline dealing with the mass collection of spatial data has developed extensively. It consists of technologies for obtaining information from the air through the use of photogrammetry and aerial laser scanning **(Nex and Remondino 2014)**. The development of automation and remote sensing systematically squeezes humans out of the direct performance of such measurements. The human contribution most often consists of the prior indication of the flight area and route together with the definition of the necessary measurement parameters such as flight altitude and data acquisition frequency **(Specht et al. 2020)**. Measurement equipment carriers (aircraft and drones) are, in many cases, equipped with INS (Inertial Navigation System) modules and modules for sensor positioning. However, due to the very high purchase cost of such high-class modules, they are most often low- and medium-

accuracy auxiliary devices. Therefore, the georeferencing of the obtained spatial data often requires corrections. With this respect, differential and static GNSS satellite measurements on ground control points (GCPs) are particularly useful. Thanks to the determination of their coordinates with the use of satellite techniques, their reliable georeferencing is obtained. Based on it, the necessary correction of photogrammetric models and point clouds is performed at the calculation stage. In many cases, surveyors performing laser scanning do not have high-end GNSS geodetic receivers with a subscription to RTK / RTN corrections. Hence, the procedure indicated in the publication is all the more valuable for them, as it indicates the way of using archival data after acquiring new spatial data enabling their georeferencing or other integration.

In view of these considerations, the existence of spatial data of various types and with various coordinate systems was stressed in this study. This property is relevant where for a given area sets of data from various sources are available. The natural consequence is that the source data must be properly transformed and brought to a homogeneous reference system. This process, called geodetic harmonization, significantly extends the possibilities of spatial analyses and concluding the processes taking place in the studied area **(Directive I. N. S. P. I. R. E. 2007)**. Throughout this article, the term "geodetic harmonization" is used to refer to the integration of geospatial data from various sources by registering them into a common coordinate reference system. Data geodetic harmonization has been the subject of research work in many scientific centres. **(Bartha and Kocsis 2011)** presented an analysis of the informative aspect of this directive **(Directive I. N. S. P. I. R. E. 2007)**, in which they discussed the structure of metadata and the standardisation procedure**. (Annoni 2011)** analysed the dependencies of the directive in the context of public institutions' access and their potential cooperation on broadly understood digitisation in its broadest sense.

(Crompvoets et al. 2008) presents a detailed discussion of geodetic harmonization procedures.

This publication is an attempt at a comprehensive summary of scientific achievements to date and presentation of the theoretical and practical aspects of data geodetic harmonization in coastal areas, where this problem occurs with increased frequency. The theoretical discussion was complemented with a practical example from the study of the tombolo phenomenon in Sopot (Poland) **(Masnicki et al. 2020)**. To illustrate the variability of the coastal area, complex measurements involving GNSS satellite measurements, laser TLS, photogrammetric UAV, and bathymetric USV measurements were made **(Specht et al. 2020**, **Masnicki et al. 2020**, **Specht et al. 2019)**. Additionally, for the analyses included in this publication, the existing archival map illustrations were used with the course of the coastline and isobates of the sea area. Terrestrial laser scanning using Trimble TX8 was performed on October 15, 2018, and included 27 sites separated in the 60-meter distance. The survey included the determination of coordinates of sphere markers using active geodetic network RTK corrections received and processed by Trimble R10 GNSS receiver. The UAV mission with DJI Mavic Pro drone was carried out at an altitude of 60 m on November 1, 2018, and resulted in taking 21 photographs used to create a point cloud with Pix4D Capture software. The bathymetric survey was performed using Navigator One AMG motorboat on October 17, 2018. The vessel was equipped in single beam SonarMite echosounder and GNSS-RTK Trimble R10 GNSS receiver.

The paper was divided into six parts. First, there is an Introduction, which presents the issues and motivation for discussing the issue topic and conducting the research. The second chapter, Materials, and Methods, describes the mathematical aspect of spatial data geodetic harmonization. The third chapter is devoted to a short

presentation of measurements of the tombolo phenomenon performed in Sopot. The fourth chapter describes practical applications of the previously discussed mathematical relationships. The fifth chapter constitutes a discussion of the obtained results. The paper ends with a Conclusions which summarizes the study.

Materials and Methods

The geodetic harmonisation procedure of spatial data obtained from measurement systems operating in different coordinate systems involves determining the values of parameters for coordinate transformation. If there are two sets of two-dimensional data with equal scale, the angle of rotation and the translation vector are the sought parameters of a single-scale affine transformation. From a numerical point of view, this aspect of geodetic harmonisation takes place in three stages. The first phase includes the adoption of one of the two spatial sets as the base. The second phase is the calculation of the value of the rotation angle around the origin of the system of coordinates. After obtaining the same directional orientation in the horizontal plane the translation vector is determined. According to the **(Bronshtein et al. 2015)**, formulas of the single-scale affine transformation are as follows:

$$x' = s[x''\cos(\theta) - y''\sin(\theta)] + \vec{T}_X$$
$$y' = s[x''\sin(\theta) + y''\cos(\theta)] + \vec{T}_Y$$

(1)

where x', y' and x'', y'' denote the coordinates of the points in the local base (X',Y') and modified (X'',Y'') system of coordinates, s denotes the scale factor, θ denotes rotation angle, and $\vec{T}_X, \vec{T}_Y$ denote planar coordinates of the translation vector.

In the study, the arithmetic mean was used to determine the estimators of the expected value of discrete random variables. This quantity is, regardless of the

distribution, a consistent and unbiased estimator of the expected value of the distribution. Additionally, if the random variable has a normal distribution, the mean is also an effective estimator. The least-squares estimator has similar features. Hence, taking into account the small size of the random sample set, the arithmetic mean was used in the calculations. The adjustment control points are defined in both local systems of coordinates and are are often characteristic, unambiguously identifiable objects in the field, e.g. clear bends in building outlines, road or pavement kerbs. Based on the designated coordinates, directional angles of selected sections are calculated in two local coordinate systems (equivalents of geodetic azimuths). Once two-directional angles have been determined, it is possible to determine the angle of rotation of one spatial set relative to another.

This algorithm can be used for both undetermined local systems as well as for system with determined orientation (e.g. cartographic mapping) **(Specht et al. 2019a)**. At this point, special attention should be paid to the orientation of axes of the coordinate system. In many cases, undetermined local coordinate systems exhibit a standard mathematical orientation of the axes of coordinate systems, i.e. the X-axis is oriented to the east and the Y-axis to the north. Coordinate systems of cartographic representations, in turn, sometimes have their axes oriented differently. For example, the Gauss-Krüger coordinate system, also known as the transverse Mercator projection, in the form defined by Gauss, has the X-axis directed to the north, while the Y-axis is directed to the east **(Deakin et al. 2010)**. The configuration of the axes causes a change in the direction in which angles grow in the coordinate system, which forces an appropriate selection of coordinates when analysing the Gauss-Krüger mathematical and cartographic coordinate systems **(Dąbrowski et al. 202)**, **Specht et al. 2019a)**.

The considerations presented above concern the geodetic harmonisation of two-

dimensional sets among others from situational geodetic measurements, orthophotomaps, or digitisation of printed maps. In the case of maps, spatial data presented in the form of graphic files require the introduction of a scale change coefficient as an additional factor. If the mapping does not provide information on coordinates, it is necessary to determine the scale change coefficient by other means. For this purpose, it is necessary to determine the actual distance between selected points on the map. Another measurement is then carried out within the raster and analogue distances corresponding to the measured distances are obtained The scale change coefficient does not affect the value of the rotation angle, but only the coordinates of points.

The geodetic harmonization of three-dimensional spatial data sets requires the previously derived formulas to be developed with an additional dimension of height. Examples of three-dimensional data include tachometric observations, bathymetric observations, point clouds from TLS **(Specht et al. 2016)**, MLS, ALS **(Vosselman and Maas 2010)** or three-dimensional photogrammetric models. These data sets consist of the basic objects in the form of points with three-dimensional coordinates. TLS point clouds and tachometric observations acquire the original data in undetermined local coordinate systems. Placing the measuring instrument on a tripod provides spatial orientation in the form of verticality and direction in the horizontal plane. On the other hand, due to the dynamic data recording, TLS and ALS point clouds and photogrammetric models require prior processing of raw measurement data for the presentation of the measured objects. For this purpose, readings from additional sensors such as GNSS receivers, accelerometers, and inclinometers are used to define the georeference of the resulting data set **(Stein 2018)**. The georeference conformity depends on the quality of the sensors used. Therefore, in low-level photogrammetry,

where low-budget UAVs are used, the georeference assigned to the objects is inaccurate. Depending on the type of navigation module and GNSS receiver used, accuracy from a few meters **(Burdziakowski and Bobkowska 2017)** to several centimetres **(Forlani et al. 2018)** can be expected.

The three-dimensional spatial datasets forces the geodetic harmonisation process to take into account not just one, but three, angles of rotation around three axes of local coordinate systems. Currently, the use of compensators neutralizing small deviations of the instrument axis from the vertical is a common standard in the construction of automated surveying instruments. When processing the recorded angles and lengths and calculating the coordinates of points, the deviation value is taken into account **(Deumlich 1982)**. Therefore, the tachometric observations and TLS point clouds generally do not require rotation around the horizontal OX and OY axes of the three-dimensional coordinate system, and only rotation around the vertical Z-axis is necessary to ensure the spatial compatibility of the data. This operation is similar to rotation in two-dimensional space, with the difference that it is necessary to take into account the transformation of the height coordinates of three-dimensional sets. To achieve this goal, depending on the scale properties of datasets, a rigid body or similarity transformation is used **(Korn and Korn 2000)**:

$$
\begin{aligned}
x' &= x''\cos(\theta) - y''\sin(\theta) + \vec{T}_X \\
y' &= x''\sin(\theta) + y''\cos(\theta) + \vec{T}_Y \ , \\
z' &= z'' + \vec{T}_Z
\end{aligned}
\tag{2}
$$

where x', y', z' denote the coordinates of the point in the local base system of coordinates (X',Y',Z'), x'', y'', z'' denote the coordinates of the point in the local

modified system of coordinates (X",Y",Z"), θ denotes rotation angle, and $\vec{T}_X, \vec{T}_Y, \vec{T}_Z$ denote three-dimensional coordinates of the translation vector.

For spatial data with a confirmed deviation of their numerical representation from the vertical, it is necessary to perform a sequence of matrix products of the corresponding rotation matrixes. The geodetic harmonisation procedure results in the spatial compatibility of the data and the correct representation of the geometry of the measured objects. Determination of the values of rotation angles around the three axes of the coordinate system has been omitted due to the complexity of the mathematical derivation. If interested, you can find the assumptions for the iterative closest point (ICP) method used, among others, in **(Besl and McKay 1992**, **Zhang 1994)**. In turn, **(Arun et al. 1987)** describe singular value decomposition (SVD), which makes it possible to determine the factoring of a symmetrical rotation matrix to a product of two rotation matrices and a scaling matrix:

$$\mathbf{R} = \mathbf{U} \cdot \mathbf{\Lambda} \cdot \mathbf{V^T} \tag{11}$$

where $\mathbf{R}$ denotes rotation matrix, $\mathbf{U}, \mathbf{V}$ denote partial rotation matrices, and $\mathbf{\Lambda}$ denotes scaling matrix.

Measurements

Verification of the presented methodological assumptions proceeded based on the results of the measurement campaign aimed at determining descriptive parameters of the tombolo phenomenon occurring in Sopot (Poland). The measurements were performed using four state-of-the-art measurement technologies: TLS, UAV photogrammetry, USV bathymetric survey with SBES echo sounder drone and differential GNSS RTK measurements. What needs to be particularly emphasized here

is that the choice of location for data geodetic harmonization analyses was not accidental, as it is located on the border of two areas (sea and land), where fundamentally different measurement techniques from two disciplines (geodesy and hydrography) are used for obtaining geospatial data. Moreover, the very high dynamics of changes of the seashore and the adjacent body of water resulting from the developing tombolo effect makes this area ideal for analyses of inconsistencies of measurement technologies and coordinate systems.

Morphological changes in the coastal zone and the shoreline course most often result from natural factors. However, they may also be the result of human activities interfering in the environment (as is the case here), where the construction of the marina has slowed down the transport of sediment along the coast, thus triggering the tombolo effect (**IO PAS 2016**). The longest European wooden pier in Sopot is regularly damaged by storms. The city authorities decided to protect the pier by building two breakwaters from the southern and eastern sides. In result, between the breakwaters and pier groyne the marina was created. The strongest surface wind waving in the Bay of Gdańsk is generated from direction N towards E. The waves hit diagonally against the shore and cause the movement of bottom sediments along the coast. The marina breakwater significantly decreased the wave energy and deflected at its ends (**Fig. 1**), which results in the formation of two vortexes. The seafloor between the marina and the shore is elevated upwards, which results in the development of a morphological formation known as a tombolo (**Mohamed 1997**). It should be stressed that this phenomenon in Sopot is unique in Poland.

Figure 1. Research site photomap (**Google Earth 2021**) and location map (**OpenStreetMap 2021**). Site coordinates: $\varphi = 54°\ 26'\ 47''$ N, $\lambda = 18°\ 34'\ 31''$ E.

A detailed presentation of the measurement procedure is outside the scope of this publication. It is recommended to consult the relevant publications describing the measurements (**Specht et al. 2020**, **Masnicki et al. 2020**, **Specht et al. 2019**). Only the basic technical parameters of the measurement equipment used, the characteristics of the obtained spatial data sets and visualisation of the measurement results are presented below. The data has been summarized in **Tab. 1**.

Table 1. Measurement technologies used to monitor the tombolo phenomenon in Sopot (Poland) and the recorded spatial data (**Geotronics 2020**, **DJI 2020**).

As a result of the measurements, a point cloud was obtained from TLS measurements, another point cloud from a photogrammetric flight pass, water depth readings along with the sounding profiles, and GNSS RTK reference points determined with centimetre accuracy. Field markers in the form of 37 spheres with a 10 cm radius were used to register (connect) the TLS point clouds. The position of selected spherical markers was determined using differential GNSS RTK technique. Corrections were obtained from commercial active geodetic GNSS network - VRSNet.pl (**Specht et al. 2017**).

The TLS points cloud had an unspecified local three-dimensional coordinate system. Thanks to the navigation module (**DJI 2020**), the cloud of UAV points received georeference in the form of coordinates of the Polish national planar PL-2000 coordinate system and ellipsoidal heights. Subsequent analyses proved a significant error in the georeferencing of the UAV point cloud. A bathymetric survey and reference measurement resulted in sets of points with flat coordinates in the national PL-2000 system and normal heights. These sets of spatial data were subjected to the geodetic

harmonization procedure to combine them and define parameters describing the tombolo phenomenon.

Data elaboration

Geodetic harmonization of the raster data set

Apart from processing the data recorded by the measurement equipment, calculations also included the geodetic harmonization of the analogue paper data set in the form of a bathymetric map. Scanning the document in high-resolution resulted in obtaining a raster data set containing, among others, isobaths in the discussed area and a grid of meridians and parallels. To make the maps, UTM was used as the coordinate system. Using formulas to convert curvilinear latitude and longitude coordinates into the flat projection coordinates presented by **(Morgaś and Kopacz 2017)**, the coordinates of intersections of the meridian and parallel images on the map were determined. Then, the corresponding coordinates were read on the raster with a map. Please note that the numerical coordinate system of the graphic data has a different axis orientation: the OX axis is oriented to the east and the OY axis to the south. The upper left corner is the origin of the raster dataset coordinate system. The coordinates in both systems are listed in **Tab. 2**.

Table 2. Coordinates of points of intersection of the images of map meridians and parallels.

The PL-2000 system, which is a Polish modification of the Gauss-Krüger projection introducing a change of scale on the axial meridian of 0.0999923 is the target system of flat coordinates for all spatial sets in the study. Axial meridian with a longitude of 18° E is relevant for Sopot and it determines the position of a zone with 3-

degree width. The UTM coordinate system is also based on a transverse cylindrical projection, but has a different coefficient of scale change on the axial meridian of 0.9996 and uses the 6°-wide latitude zones. In Sopot, the 21° E meridian is relevant for UTM. The image of Sopot on maps in both coordinate systems can be found on the opposite sides of the zone central meridian: on the right in PL-2000 and on the left in UTM. As a result, projections of meridians show convergence in opposite directions. For this reason, it is not possible to use a simple map translation procedure in the UTM system into the PL-2000 target system. Geodetic harmonization of the raster set requires the use of further affine transformations modifying the form of the raster set to be completed. Due to the limited volume of this paper, only calculations transforming the raster coordinates into coordinates in the UTM system will be presented.

Based on the coordinates of points in both coordinate systems, the coefficient of scale change was determined. After multiplying the coordinates read from the raster set by the scale coefficient , a metric numerical map was obtained. In this case, there was no rotation because the values of directional angles between characteristic points were very similar in both systems. The next geodetic harmonization stage thus only included the determination of the coordinates of the **T** translation vector transforming the entire raster set to the coordinates of the UTM system. The following calculation steps are presented in **Tab. 3**.

Table 3. Determination of scale change coefficient and translation vector of the raster dataset.

Geodetic harmonization of TLS point cloud

The initial stage of processing point clouds includes registration, which allows for combining scans from adjacent sites into one point cloud **(Vosselman and Maas 2010)**.

They are recorded by identifying the same objects in individual scans and then

performing the transformation. The registration error of 27 point clouds based on

spherical markers was 2.5 mm. The resulting point cloud had an undetermined local

coordinate system from the first measurement station. The extreme and middle markers

were selected for georeferencing of TLS point clouds. As a result of GNSS RTK

measurements, flat coordinates of the 8 spheres in the PL-2000 system and height in the

normal height system were obtained (**Tab. 4**, **Fig. 2**).

Table 4. Coordinates of spherical TLS markers in primary and secondary systems.

Figure 2. Location of markers for point clouds registration (blue) with an indication of

selected spheres used for georeferencing (green).

Based on coordinates of spheres in both coordinate systems, metric control of

both the TLS point cloud and the obtained results of GNSS RTK reference

measurements was performed. For five selected distances between the spheres, a scale

change coefficient of 1.0001 with a standard deviation of 0.0005 was obtained. The

analysis proved that both sets of data have a similar linear scale. On this basis, it was

assumed that the coefficient of scale change is s = 1. Next, the values of directional

angles and the angle of rotation were calculated. At each measuring station, the Trimble

TX-8 laser scanner was levelled, so the only considered elementary rotation of the TLS

point cloud was the rotation around the OZ vertical axis. The values of directional

angles, partial rotation angles and the final rotation angle are shown in **Tab. 5**.

Table 5. Coordinates of spherical markers in primary and secondary systems.

The value of the angle of rotation was determined with a standard deviation of 0° 0' 06.4". This demonstrates the high accuracy of both the calculations and the source coordinates in both coordinate systems. Thanks to levelling of the laser scanner and the use of instrument's compensator there was no need for additional rotations around the horizontal axes of the coordinate system. The rotation matrix of the necessary rotation around the OZ axis has the form presented in **Tab. 6**.

Table 6. Matrix of rotation around the Z-axis by an angle of rotation θ.

Another stage of geodetic harmonization included the determination of the coordinates of the translation vector. Once all the markers were rotated, the increments were calculated between coordinates in the primary and secondary system. Then, with a set of data accordingly directed in the horizontal plane, the coordinates differences were determined between the rotated points in the local system and the points in the PL-2000 coordinate system. **Tab. 7** presents the process of calculating the translation vector.

Table 7. Coordinates of the rotated control points, reference points, and translation vector.

Standard deviations of the individual coordinates of the vector T_x, T_y, T_z were 0.012, 0.018, and 0.019 m, respectively. With a set of necessary data being complete, i.e. with the rotation matrix and the translation vector, the procedure of harmonizing the TLS point cloud in the local system to the PL-2000 system was performed. In accordance with the principles observed in all geodetic surveys, after calculating the coordinates of characteristic points, the values of their coordinates were compared with

those from the GNSS RTK measurement. The results of the accuracy analysis are presented in **Tab. 8**.

Table 8. The coordinates of control points after geodetic harmonisation and their differences with respect to the coordinates of reference points.

The resulting deviation values show geodetic harmonization error in a horizontal plane not exceeding 0.016 m. In the vertical plane, the maximum deviation is 0.027 m. The results of the geodetic harmonization of the TLS point cloud are presented in graphical form in **Fig. 3**. The left side of the drawing contains the original spatial data set. The right side of the drawing shows the TLS point cloud after geodetic harmonization and bringing it to the desired coordinate system.

Figure 3. TLS cloud in the local undetermined system (a) and in the PL-2000 system (b) – top view. Green and blue markers are spheres used to point clouds registration (blue) and geodetic harmonisation (green).

The local TLS cloud coordinate system resulted from adopting the coordinate system of the first measurement station as global for the whole recorded cloud. The origin of the coordinate system was at the emission-receiving centre of the laser scanner, while the alignment of the OX' and OY' axes resulted from the way the instrument was attached to the levelling head. The rotation and translation defined by the determined matrix coefficients made it possible to make the TLS data set compatible with the national PL-2000 system and normal height system. The arithmetic mean of the

deviations on the adjustment points usually serves as the estimator of the geodetic harmonization error (**Tab. 8**).

Geodetic harmonization of UAV point cloud

Another set of spatial data undergoing the geodetic harmonization process was a point cloud generated from the photogrammetric model. The point cloud had a georeference coming from UAV navigation sensors of the DJI Mavic Pro drone, but after comparing it with the harmonized TLS point cloud it turned out that the UAV georeference is inaccurate. For geodetic harmonization, its georeference had to be corrected to the true coordinates of the PL-2000 plane system and the normal height system. Due to the georeference accuracy, its detailness and resolution, the TLS cloud was used as a reference object in relation to the UAV cloud. To determine transformation parameters from both point clouds, the coordinates of corresponding points were indicated (**Tab. 9**).

Table 9. Coordinates of control points for geodetic harmonisation of UAV point cloud.

At the stage of displaying and processing spatial data, it seems justified to introduce a fixed offset to reduce large coordinate values. In this case, an offset vector with coordinates $\mathbf{V_{OFF}}^{\mathbf{T}}$ = [-6537000 m, -6035000 m, 0 m] was used. The analysis of linear dependencies of the ICP method proved that spatial sets of both point clouds exhibit a scale difference. Therefore, a scale change coefficient with a non-unitary value could be found in the rotation matrix. The rotation matrix harmonizing the UAV cloud had the following form (**Tab. 10**):

Table 10. Rotation matrix of the UAV cloud.

Lack of zero and unitary elements in the rotation matrix is indicative of a couple of partial rotations, which must be performed to correct the georeference of the UAV point cloud. The application of the SVD method resulted in the following components of the U, V T rotation matrix, and the Λ scaling matrix (**Tab. 11**):

Table 11. SVD distribution of the UAV cloud rotation matrix.

Angles of rotation around the OX, OY, OZ axes of the coordinate system determined from the partial rotation matrices $\mathbf{U}$, $\mathbf{V}^\mathbf{T}$ take the following values: -42° 10' 28.4", 89° 32' 39.9", -132° 10' 3.5" (**U** matrix) and -90° 24' 49.4", -0° 0' 16.6", 90° 11' 21.9" ($\mathbf{V}^\mathbf{T}$ matrix). After the first partial rotation using the $\mathbf{V}^\mathbf{T}$ matrix, the UAV point cloud was subjected to a scale change of $s = 0.976309$ and then rotated with the values in the $\mathbf{U}$ matrix. The last calculation stage included the determination of the translation vector by which the rotated point cloud should be shifted. Four points used for spatial transformation adjustment were rotated according to the matrix values (Tab. 6). In the matrix form, the spatial operation of rotation taking into account the $\mathbf{V_{OFF}}$ offset vector is expressed by the following formula:

$$\mathbf{P^I} = \mathbf{U} \cdot \mathbf{\Lambda} \cdot \mathbf{V^T} \cdot \left(\mathbf{P^{II}} + \mathbf{V_{OFF}}\right) - \mathbf{V_{OFF}} \tag{4}$$

where $\mathbf{P^I}$ denotes the coordinates of the adjustment point in the corrected coordinate system, and $\mathbf{P^{II}}$ denotes coordinates of the adjustment point of the corrected coordinate system after rotation.

The coordinates of adjustment geodetic harmonization of the UAV point cloud points before and after rotation are shown in **Tab. 12**.

Table 12. SVD distribution of the UAV cloud rotation matrix.

After comparing the coordinates of rotated points in the modified coordinate system of the UAV point cloud and their corresponding coordinates in the target system of harmonized spatial sets, the translation vector with the coordinates $\mathbf{T}^T = [1.175, 3.850, 53.639]$ was determined. The described case is connected to the occurrence of the multi-rotational rotation matrix, which is a generalisation of the simplified variant indicated in formula (1).

Geodetic harmonization of bathymetric data

Coordinates from differential GNSS RTK measurements were assigned to bathymetric data containing depths and recorded during the survey of the area surrounding the pier in Sopot. In this study, a reference station of the VRS Net.pl network located in Gdańsk was used. Therefore, there was no need to perform additional mathematical operations to harmonise the data. The depth recorded by the echo sounder obtained the positional data in the target coordinate system.

Results and discussion

The mathematical relationships presented in the theoretical Materials and Methods section were applied to real spatial data. The Polish national PL-2000 plane coordinate system and normal height system are target coordinate systems for the whole geodetic harmonization process. In the study, a precise satellite GNSS RTK positioning method was used to determine reference values based on which the necessary transformation

parameters were determined. Point coordinates were used to modify the original

coordinate systems of spatial data coming from the bathymetric map and measurements.

The obtained deviation values prove the accuracy of the geodetic harmonization

process for individual data set down to three centimetres. The results of these operations

are presented in **Fig. 4**.

Figure 4. The result of geodetic harmonisation of spatial data used in the study of the

tombolo phenomenon in Sopot.

Both parts of **Fig. 4** are views in the same viewer-based perspective. To avoid

overlapping of points from TLS and UAV point clouds, they are presented separately

with the bathymetric map described in section 4.1. **Fig. 4a**, except for the TLS point

cloud transformed from the local system into the PL-2000 and the normal height

systems (section 4.2), contains locations (marked in green) of points used for

georeferencing and blue marked locations of spheres used for registration the TLS point

cloud. In addition, the top figure includes bathymetric profiles measured by the

unmanned vessel. **Fig. 4b** presents a UAV point cloud with corrected georeference of

the PL-2000 system. Thanks to the appropriate application of transformation

procedures, all the spatial data presented above have been unified and brought to a

single spatial system, which is the essence of the geometric aspect of geodetic

harmonization.

The conducted research presents the subject of harmonization of spatial data sets

in a different way than the research by other authors. Starting from the guidelines of the

I.N.S.P.I.R.E. directive, numerous authors discussed the procedures of standardization

and unification of the description and storage of spatial data. The development of a

uniform method of data tagging is conducive to their rapid spatial identification and

potential use by users. Other researchers focused on the aspect of spatial data

management at the local and supranational level and pointed to the legitimacy of

creating advanced spatial databases. The development of mechanisms enabling

cooperation and data exchange between centers from different countries and centers is

conducive to the development of science and the carrying out of complex geospatial and

statistical analyzes. The presented research results, unlike the above-mentioned ones,

focus on the presentation of a practical procedure for processing spatial data. The

conducted measurement campaign provided a valuable and diverse set of data to show

the numerical aspects of the harmonization process.

The limitation of this study was the assessment of the final (total) accuracy of

the harmonized spatial data. The study is continued with the ongoing research taking

into account sensor errors and spatial data processing methods, e.g. TLS point cloud

registration. The research uses, among others Gaussian Error Propagation model. The

results of the study will be presented in a separate publication. A schematic outline of

the research problem is shown in **Fig. 5**. From the analytical point of view, the final

harmonized data error value will be determined from the relationship:

$$m_{GH} = \sqrt{m_{TLS}^2 + m_{UAV}^2 + m_{GNSS}^2 + m_{map}^2 + m_{SBES}^2} \,, \tag{5}$$

where subscripts denote the following errors: GH - geodetic harmonization, TLS -

terrestrial laser scanning point cloud, UAV - unmanned aerial vehicle point cloud,

GNSS – ground reference points (GCPs), SBES - bathymetric data, and map - raster

map.

Figure 5. Factors influencing the total error of geodetic harmonization (GH) of a spatial

data set.

Conclusions

The rapid development of mass data acquisition methods and a large number of archive studies constitute a challenge for joint use. Achieving internal cohesion in spatial data with a varied number of dimensions constitutes a significant direction for the development of spatial analysis. Numerical data formats and coordinate systems assigned to them are different, which results in the need to develop a methodology for determining the transformation parameters for individual spatial data sets. This issue is a subject of consideration of both scientists and governments. European legislation has addressed this issue by establishing a geodetic harmonization procedure. This paper discusses the geometric aspect of geodetic harmonization and presents research results based on both theoretical aspects and practical verification of the methodology.

In the theoretical part, the mathematical procedures used in the process of spatial data geodetic harmonization are described. Furthermore, they are indicative of the importance of the process of identifying and obtaining coordinates of corresponding points in datasets with different coordinate systems. The presented mathematical model was verified with real data. The research material comes from a measurement campaign conducted to determine descriptive parameters for the tombolo phenomenon in Sopot. The results of differential GNSS RTK measurements, terrestrial laser scanning, bathymetric survey, photogrammetry and an analogue archival bathymetric map were used in the study. Due to the measurement methods used and differences in coordinate systems, the data presented valuable material for demonstrating the practical aspects of geodetic harmonization. The errors obtained for individual data sets did not exceed three centimetres, which confirms the effectiveness of the presented geodetic harmonization procedure.

Declaration of interest statement

The authors declare that they have no known competing financial interests or personal

relationships that could have appeared to influence the work reported in this paper.

References

Annoni, A. 2011. "INSPIRE and the digital agenda for Europe." *Roczniki Geomatyki,* Vol. 9 (No. 5): pp. 7-16.

Arun, K.S., Huang, T.S. and Blostein, S.D. 1987. "Least-squares fitting of two 3-D point sets." *IEEE Transactions on pattern analysis and machine intelligence*, Vol. 5: pp. 698-700.

Bagrow, L. 2010. *History of cartography*. New Brunswick, NJ: Transaction publishers.

Bartha, G. and Kocsis, S. 2011. "Standardization of geographic data: The European inspire directive." *European Journal of Geography*, Vol. 2(No. 2): pp. 79-89.

Besl, P.J., and McKay, N.D. 1992. "Method for registration of 3-D shapes." Paper presented at Sensor fusion IV: control paradigms and data structures, April 1992.

Bronshtein, I.N., Semendyayev, K.A., Musiol, G., and Mühlig, H. 2015. *Handbook of Mathematics, Sixth Edition*. Berlin Heidelberg: Springer-Verlag.

Bugayevskiy, L.M., and Snyder, J. 2013. *Map projections: A reference manual*. Boca Raton, FL: CRC Press.

Crompvoets, J., Rajabifard, A., van Loenen, B., and Fernández, T.D. 2008. *A multi-view framework to assess Spatial Data Infrastructures*. Melbourne: Digital Print Centre, The University of Melbourne.

Dąbrowski, P.S., Specht, C., Felski, A., Koc, W., Wilk, A., Czaplewski, K., Karwowski, K., et al. 2020. "The Accuracy of a Marine Satellite Compass under Terrestrial Urban Conditions." *Journal of Marine Science and Engineering*, Vol. 8 (No. 1): p. 18. doi: 10.3390/jmse8010018.

Dąbrowski, P.S., Specht, C., Koc, W., Wilk, A., Czaplewski, K., Karwowski, K., Specht, M., Chrostowski, P., Szmagliński, J., and Grulkowski, S. 2019. "Installation of GNSS receivers on a mobile railway platform–methodology and measurement aspects." *Scientific Journals of the Maritime University of Szczecin*, Vol. 60: pp. 18-26. doi: 10.17402/367.

Deakin, R.E., Hunter, M.N., and Karney, C.F.F. 2010. "The Gauss-Krüger projection." Paper presented at 23rd Victorian regional survey conference, Warrnambool, Australia, September 2010.

Deumlich, F. 1982. *Surveying instruments*. Berlin, New York: Walter de Gruyter.

Directive I. N. S. P. I. R. E. 2007. "Directive 2007/2/EC of the European Parliament and of the Council of 14 March 2007 establishing an Infrastructure for Spatial Information in the European

Community (INSPIRE)". *EUR-Lex*, last modified 26/06/2019, https://eur-lex.europa.eu/legal-content/EN/ALL/?uri=CELEX:32007L0002.

DJI 2020. "Mavic Pro - DJI." *DJI - Official Website*, last modified 18/3/2020, https://www.dji.com/pl/mavic.

Geotronics 2020. "Produkty i rozwiązania." *Geotronics Dystrybucja*, last modified 18/3/2020, https://www/geotronics.com.pl.

Google Earth Pro 2021. "Google Earth Pro V 7.1.8.3036. Sopot, Poland. 54 26'47"N 18 34'35"E, Eye altitude 770 m." *Google*, last modified 18/03/2020, https://www.google.pl/intl/pl/earth/.

Hofmann-Wellenhof, B., Legat, K., and Wieser, M. 2003. *Navigation*. Wien: Springer Science & Business Media.

IO PAS 2016. "Conducting Research and Modeling of the Seafloor and Sea Shore Near the Pier in Sopot." *Institute of Oceanology of the Polish Academy of Sciences.* last modified 9/6/2019, https://bip.umsopot.nv.pl/Download/get/id,32756.html.

Korn, G.A., and Korn, T.M. 2000. *Mathematical handbook for scientists and engineers: definitions, theorems, and formulas for reference and review*. Mineola, NY: Dover Publications, INC.

Krynski, J., Rogowski, J.B., and Liwosz, T. 2019. "Research on reference frames and reference networks in Poland in 2015–2018." *Geodesy and Cartography*, Vol. 68 (No. 1): pp. 5-29. doi: 10.24425/gac.2019.126093.

Maling, D.H. 1992. *Coordinate systems and map projections, Second Edition*. Oxford, New York, Seoul, Tokyo: Pergamon Press.

Masnicki, R., Specht, C., Mindykowski, J., Dąbrowski, P., and Specht, M. 2020. "Accuracy analysis of measuring XYZ coordinates with regard to the investigation of the tombolo effect." *Sensors*, Vol. 20 (No. 4): p. 1167. doi: 10.3390/s20041167.

Mohamed, A.S. 1997. *2D and 1D numerical model simulations for the effect of a single detached breakwater on the shore*. MSc Thesis, Delft: Delft University of Technology.

Morgaś, W., and Kopacz, Z. 2017. "Conversion of geodetic coordinates into flat (2-dimensinal) coordinates PL-UTM for the purposes of navigation." *Scientific Journal of Polish Naval Academy*, Vol. 208 (No. 1): pp. 45-60.

Nex, F., and Remondino, F. 2014. "UAV for 3D mapping applications: a review." *Applied geomatics*, Vol. 6 (No. 1): pp. 1-15.

OpenStreetMap 2021. "OpenStreetMap." *OpenStreetMap*, last modified 13/3/2021, https://www.openstreetmap.org.

Robinson, A., Sale, R., and Morrison, J. 1978. *Elements of Cartography*. New York: John Wiley & Sons, Inc.

Smith, J.R. 1997. *Introduction to geodesy: the history and concepts of modern geodesy (Vol. 1)*. Hoboken, NJ: John Wiley & Sons.

Specht, C., Dabrowski, P.S., Pawelski, J., Specht, M., and Szot, T. 2019. "Comparative analysis of positioning accuracy of GNSS receivers of Samsung Galaxy smartphones in marine dynamic measurements." *Advances in Space Research*, Vol. 63 (No. 9): pp. 3018-3028. doi: 10.1016/j.asr.2018.05.019.

Specht, C., Dąbrowski, P., Dumalski, A., and Hejbudzka, K. 2016. "Modeling 3D Objects for Navigation Purposes Using Laser Scanning." *TransNav: International Journal on Marine Navigation and Safety of Sea Transportation*, Vol. 10 (No. 2): pp. 301-306. doi: 10.12716/1001.10.02.12.

Specht, C., Specht, M., and Dąbrowski, P. 2017. "Comparative analysis of active geodetic networks in Poland." Paper presented at International Multidisciplinary Scientific GeoConference: SGEM: Surveying Geology & mining Ecology Management, Prague, Czech Republic, June-July 2017. doi: 10.5593/sgem2017/22/S09.021.

Specht, M., Specht, C., Lasota, H., and Cywiński, P. 2019. "Assessment of the Steering Precision of a Hydrographic Unmanned Surface Vessel (USV) along Sounding Profiles Using a Low-Cost Multi-Global Navigation Satellite System (GNSS) Receiver Supported Autopilot." *Sensors*, Vol. 19 (No. 18): p. 3939. doi: 10.3390/s19183939.

Specht, M., Specht, C., Mindykowski, J., Dąbrowski, P., Maśnicki, R., and Makar, A. 2020. "Geospatial Modeling of the Tombolo Phenomenon in Sopot using Integrated Geodetic and Hydrographic Measurement Methods." *Remote Sensing*, Vol. 12 (No. 4): p. 737. doi: 10.3390/rs12040737.

Stein, D. 2018. *Mobile laser scanning based determination of railway network topology and branching direction on turnouts (Vol. 38)*. Karlsruhe: KIT Scientific Publishing.

Torge, W., and Müller, J. 2012. *Geodesy*. Berlin, Boston: Walter de Gruyter.

Visvalingam, M. 1990. "Trends and concerns in digital cartography." *Computer-Aided Design*, Vol. 22 (No. 3): pp. 115-130.

Vosselman, G., and Maas, H.G. 2010. *Airborne and terrestrial laser scanning*. Boca Raton, FL: CRC press.

Yang, Q., Snyder, J., and Tobler, W. 1999. *Map projection transformation: principles and applications*. Boca Raton, FL: CRC Press.

Zhang, Z. 1994. "Iterative point matching for registration of free-form curves and surfaces." *International journal of computer vision*, Vol. 13 (No. 2): pp. 119-152.

Table 1. Measurement technologies used to monitor the tombolo phenomenon in Sopot (Poland) and the recorded spatial data **(Geotronics 2020, DJI 2020)**.
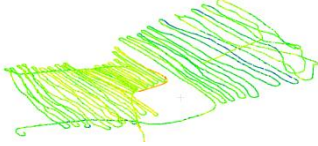
Measurement technology	Measurement equipment	Spatial data
TLS	Trimble TX-8 Time-of-flight laser scanner	Point cloud
UAV	DJI Mavic Pro Multi-rotor drone with camera and GPS/GLONASS positioning	Point cloud
RTK GNSS	Trimble R10 Multi-GNSS receiver	Reference points
USV + RTK GNSS + SBES	HyDrone + SonarMite + Trimble R10 Remote control vessel with GNSS receiver and single-beam echosounder	Bathymetric survey

Table 2. Coordinates of points of intersection of the images of map meridians and parallels.

No	Raster		UTM	
	x [pix]	y [pix]	Nothing [m]	Easting [m]
1	5509	13148	6035931.394	342656.010
2	10613	13324	6035923.949	342872.101
3	15717	13498	6035916.514	343088.191
4	5811	4388	6036302.182	342668.795
5	10915	4564	6036294.737	342884.867
6	16019	4738	6036287.303	343100.940

Table 3. Determination of scale change coefficient and translation vector of the raster dataset.

	Raster distance [pix]	UTM distance [m]	s [m/pix]	Raster scaled		Translation vector	
				x [m]	y [m]	Easting [m]	Northing [m]
-	-	-	-	233.228	556.631	342422.783	6036488.025
d $_{1-2}$	5107.034	216.218	0.042337381	449.310	564.082	342422.791	6036488.031
d $_{1-3}$	10213.998	432.436	0.042337631	665.392	571.448	342422.799	6036487.962
-	-	-	-	246.013	185.769	342422.782	6036487.952
d $_{4-5}$	5107.034	216.201	0.042333934	462.095	193.221	342422.772	6036487.958
d $_{4-6}$	10213.998	432.401	0.042334194	678.177	200.587	342422.763	6036487.890
		s =	0.042335785		mean =	342422.782	6036487.969
					std =	0.012	0.048

Table 4. Coordinates of spherical TLS markers in primary and secondary systems.

No	Local TLS Coordinate System			PL-2000 system		Normal height [m]
	x' [m]	y' [m]	z' [m]	Easting [m]	Nothing [m]	
1	5.625	-58.129	-1.980	6537207.845	6035148.375	1.136
2	22.044	-36.590	-2.140	6537183.163	6035137.275	0.977
3	38.010	-16.104	-1.620	6537159.353	6035126.877	1.483
4	192.181	-184.240	-1.810	6537103.942	6035348.151	1.278
5	199.701	-165.421	-1.740	6537088.359	6035335.190	1.351
6	452.511	-305.242	-1.630	6536932.782	6035578.575	1.447
7	462.537	-292.243	-1.910	6536917.772	6035571.923	1.159
8	471.434	-279.343	-1.230	6536903.786	6035564.824	1.834

Table 5. Coordinates of spherical markers in primary and secondary systems.

No	Directional angle		Angle of rotation
	Primary system (TLS)	Secondary system (PL-2000)	
1	-28° 56' 28.1"	122° 35' 39.1"	151° 32' 07.2"
2	-30° 07' 48.0"	121° 24' 27.9"	151° 32' 15.9"
3	-31° 16' 20.3"	120° 15' 57.6"	151° 32' 17.9"
4	-24° 55' 44.8"	126° 36' 18.5"	151° 32' 03.3"
5	-25° 45' 28.6"	125° 46' 33.9"	151° 32' 02.5"
		$\theta =$	**151° 32' 09.3"**

Table 6. Matrix of rotation around the Z-axis by an angle of rotation θ.

-0.87911614	-0.47660761	0
0.47660761	-0.87911614	0
0	0	1

Table 7. Coordinates of the rotated control points, reference points, and translation vector.

No	Rotated TLS			Translation vector		
	x' [m]	y' [m]	z' [m]	T_x [m]	T_y [m]	T_z [m]
1	22.760	53.783	-1.980	6537185.085	6035094.592	3.116
2	-1.940	42.673	-2.140	6537185.103	6035094.602	3.117
3	-25.740	32.273	-1.620	6537185.093	6035094.604	3.103
4	-81.139	253.563	-1.810	6537185.081	6035094.588	3.088
5	-96.719	240.603	-1.740	6537185.078	6035094.587	3.091
6	-252.329	484.013	-1.630	6537185.111	6035094.562	3.077
7	-267.339	477.364	-1.910	6537185.111	6035094.559	3.069
8	-281.308	470.264	-1.230	6537185.094	6035094.560	3.064
				6537185.095	**6035094.582**	**3.091**

Table 8. Coordinates of the rotated control points, reference points, and translation vector.

No	Easting [m]	Nothing [m]	Normal height [m]	dE [1] [m]	dN [2] [m]	dHn [3] [m]
1	6537207.854	6035148.365	1.111	0.009	-0.010	-0.025
2	6537183.154	6035137.255	0.951	-0.009	-0.020	-0.026
3	6537159.355	6035126.855	1.471	0.002	-0.022	-0.012
4	6537103.955	6035348.145	1.281	0.013	-0.006	0.003
5	6537088.375	6035335.185	1.351	0.016	-0.005	0.000
6	6536932.766	6035578.595	1.461	-0.016	0.020	0.014
7	6536917.756	6035571.946	1.181	-0.016	0.023	0.022
8	6536903.786	6035564.846	1.861	0.000	0.022	0.027

[1, 2, 3] dE, dN, and dHn - difference in easting, northing and normal height coordinates with respect to reference points.

Table 9. Coordinates of control points for geodetic harmonization of UAV point cloud.

No	UAV point cloud			TLS point cloud		
	Easting [m]	Northing [m]	Normal height [m]	Easting [m]	Northing [m]	Normal height [m]
1	6537211.199	6034995.216	-51.774	6537207.268	6034998.526	2.738
2	6537245.721	6035038.053	-52.937	6537240.967	6035040.331	0.986
3	6536878.170	6035669.089	-43.590	6536882.100	6035656.468	2.761
4	6536795.179	6035676.733	-41.043	6536801.079	6035663.959	5.314

Table 10. Rotation matrix of the UAV cloud.

9.76307154E-01	-6.89628000E-05	1.98299368E-03
4.29534080E-05	9.76225197E-01	1.28026186E-02
-1.98372732E-03	-1.28025049E-02	9.76223230E-01

Table 11. SVD distribution of the UAV cloud rotation matrix.

|			
U =	-5.33763447E-03	9.99985745E-01	1.36281055E-04
	-5.89327382E-03	1.04824041E-04	-9.99982629E-01
	-9.99968389E-01	-5.33834489E-03	5.89263030E-03
V^T =	-3.30608301E-03	7.22036216E-03	-9.99968468E-01
	9.99994532E-01	1.04182407E-04	-3.30541693E-03
	8.03128149E-05	-9.99973927E-01	-7.22066711E-03
Λ =	0.9763092	0	0
	0	0.9763092	0
	0	0	0.9763091

Table 12. Coordinates of the UAV point cloud geodetic harmonization control points.

| No	Easting [m]	Northing [m]	Normal height [m]	Easting [m]	Northing [m]	Normal height [m]
		Before			After	
1	6537211.199	6034995.216	-51.774	6537206.093	6034994.676	-50.901
2	6537245.721	6035038.053	-52.937	6537239.792	6035036.481	-52.653
3	6536878.170	6035669.089	-43.590	6536880.924	6035652.618	-50.878
4	6536795.179	6035676.733	-41.043	6536799.904	6035660.110	-48.325

Figure 1. Research site photomap **(Google Earth 2021)** and location map **(OpenStreetMap 2021)**. Site coordinates: $\varphi = 54°\ 26'\ 47''$ N, $\lambda = 18°\ 34'\ 31''$ E.
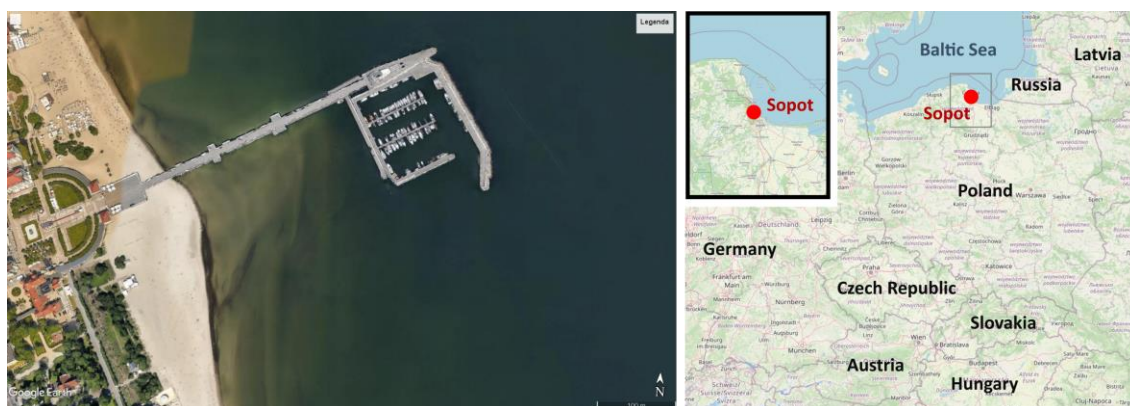
Figure 2. Location of markers for point clouds registration (blue) with an indication of selected spheres used for georeferencing (green).
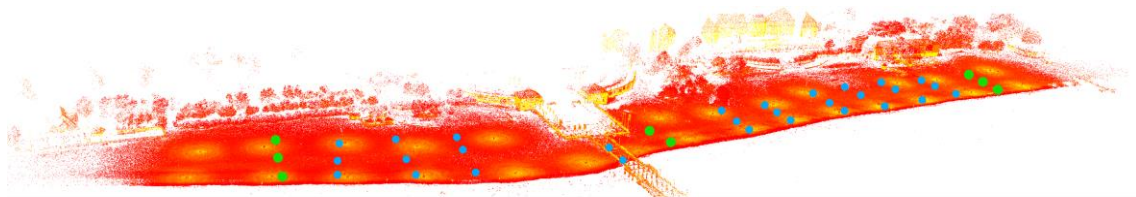
Figure 3. TLS cloud in the local undetermined system (a) and in the PL-2000 system (b) – top view. Green and blue markers are spheres used to point clouds registration (blue) and geodetic harmonization (green).

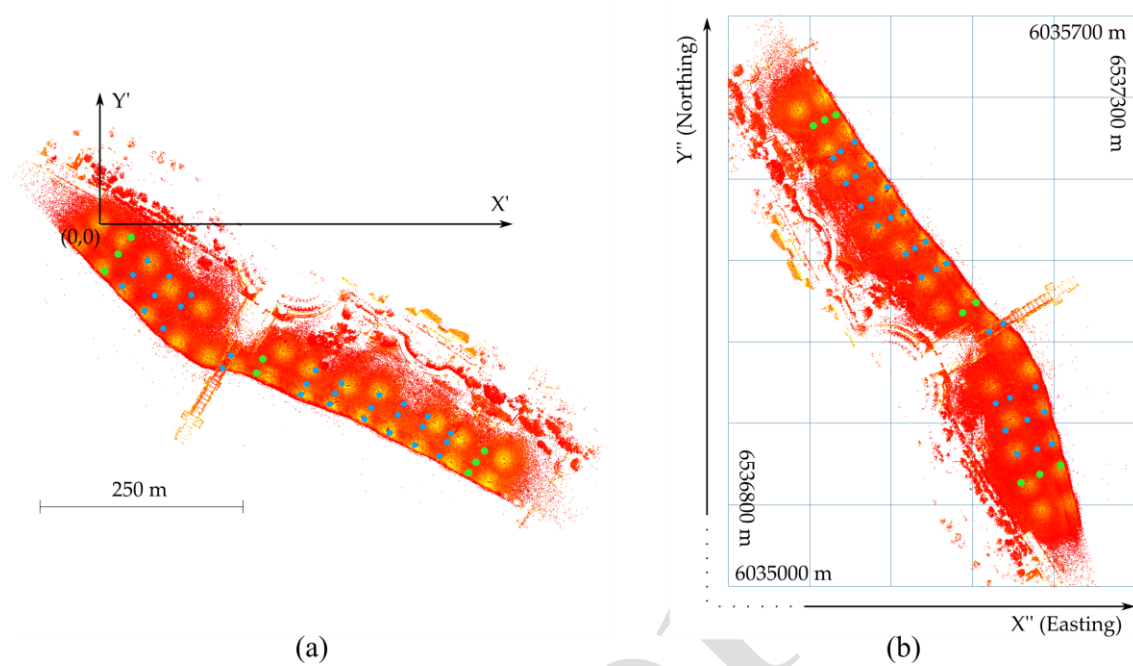(a)   (b)

Figure 4. The result of geodetic harmonization of spatial data used in the study of the tombolo phenomenon in Sopot.
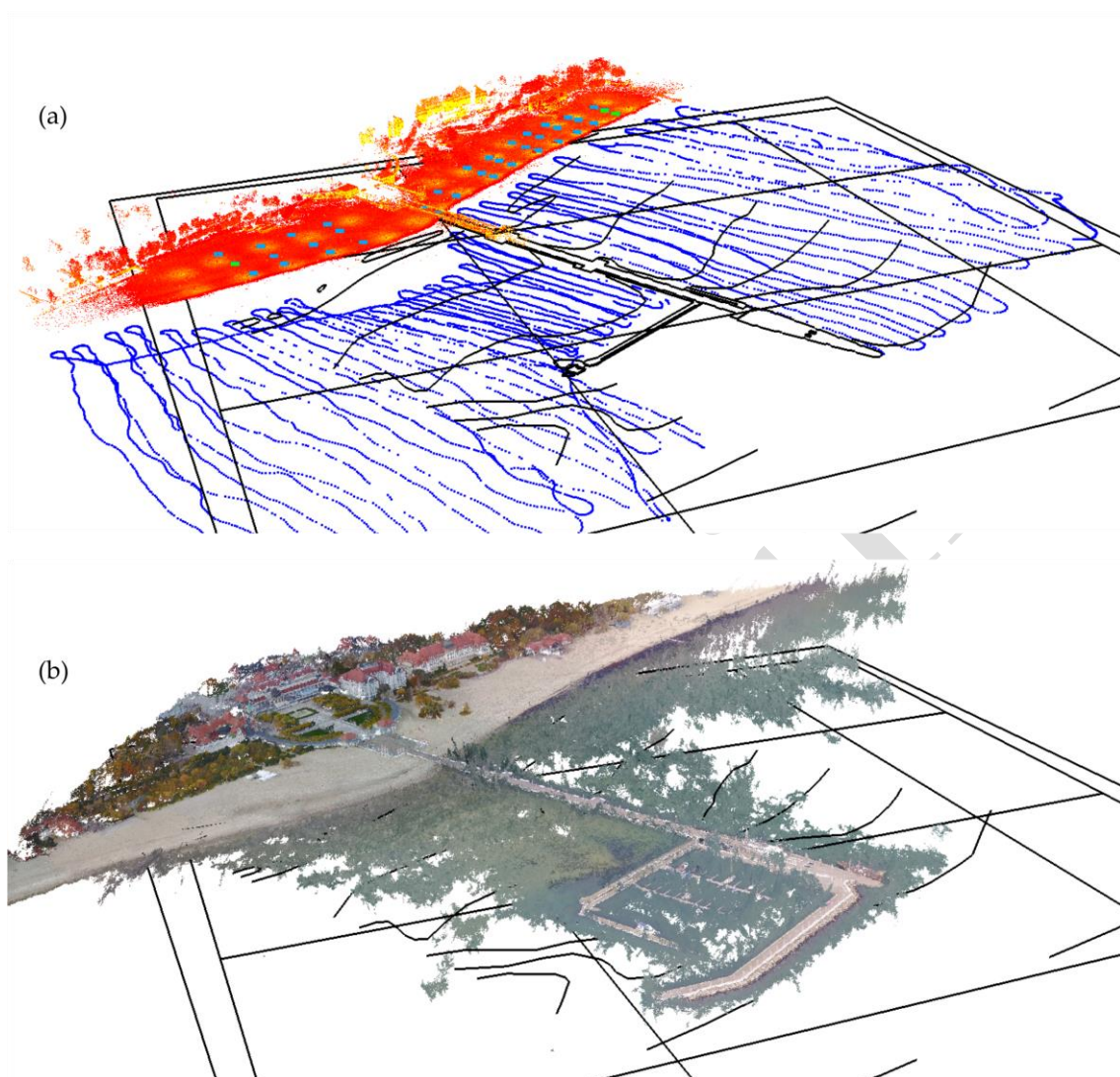
Figure 5. Factors influencing the total error of geodetic harmonization (GH) of a spatial data set.